Hidden state dynamics reveals metastability across the adult lifespan

Keyu Chen[1], Qing Wang[1], Dong-Qiang Liu[1*]

[1]Research center of Brain and Cognitive Neuroscience, Liaoning Normal University, Dalian, China

Abstract

Adult lifespan is accompanied by functional reorganization of brain networks, but the dynamic patterns behind this reorganization remain largely unclear. This study focuses on modelling the time-varying process of spontaneous activity of large-scale networks using hidden Markov model (HMM), and investigates how it changes with age. The HMM with 12 hidden states was applied to temporally concatenated resting state fMRI data of 422 subjects (aged 19-80 years), and each hidden state was characterized by distinct activation patterns of 17 brain networks. Results showed that (a) the elder were probable to spend more time on an 'inactive' state with only mean-level activation of all networks. (b) The elder tended to spend less time on states showing antagonistic activity between various pairs of networks including default mode network, control and salience/ventral attention networks. (c) The transition probabilities between certain pairs of states that default mode or control networks showed opposite activation level exhibited significant increases/decreases with age. (d) Lifespan trajectories of subjects' fractional occupancy and transition probability exhibited U-shaped or linear trends. These results demonstrated that the particular network state with lower transition probability and higher fractional occupancy in old cohort could be detected using HMM, and proved that HMM is a huge potential tool to reveal the metastability, the ability of the system to transition between different cognitive states, across the adult lifespan.

Key words: life span; hidden markov model; resting state fMRI

1.Introduction

Accumulating evidence has demonstrated that human brain undergoes structural and functional changes across the whole lifespan (Grady et al., 2006; Riddle et al., 2010;

Vannest et al., 2015; Kennedy et al., 2017; Narvacan et al., 2017). These functional changes between large-scale networks could be investigated using resting-state fMRI (Biswal et al., 1995; Grecius et al., 2003; Fox and Raichle, 2007). Although a multitude of studies have unveiled the lifespan changes in functional networks (Chan et al., 2014; Betzel et al., 2014; Yang et al., 2014; Finotelli et al., 2018) via static functional connectivity, the underlying dynamic processes of the human brain across the adult lifespan are poorly understood. In recent years, methods such as dynamic functional connectivity (dFC) based on sliding windows approach (Allen et al., 2014) and co-activation patterns (CAPs, Liu et al., 2013) suggested that the resting brain activity are highly dynamic and could be clustered into discrete and recurring 'states'. Statistics like dwell time (proportion of time spent visiting each state) and transition probability (the frequency of transition between a pair of states) were also introduced to measure specific network dynamics of some brain disorders like schizophrenia (Rashid et al., 2014; Damaraju et al., 2014; Rabany et al., 2019), Parkinson's (Kim et al., 2017; Zhuang et al., 2018; Diez-Cirarda et al., 2018;) and Alzheimer's (De Vos et al., 2018; Fu et al., 2019; Schumacher et al., 2019) However, it remains rarely known regarding how such 'switching dynamics' (e.g. transition probability) changes with age. Naik et al. (2017) suggested the complexity of brain dynamic processes in aging is better understood using the concept of metastability (the ability of the system to transit between different cognitive states), and expected that lower transition probability and/or higher dwell time would be found in the old cohort. Although a few previous studies have discovered that the dwell time of some FC states with weak interactions (Tian et al., 2018) or negative connectivity (Xia et al., 2019) throughout the brain was longer in elderly, and the transition probabilities of specific FC states between three age groups (young, adult and old) were also different (Chen et al., 2018), the relationship between metastability and adult lifespan has not been fully understood. One of the important reasons is that the aforementioned dFC studies employed sliding window approaches which suffers from a number of severe limitations such as window length (Hindriks et al., 2016; Leonardi & Van De Ville, 2015) and extent of overlap (Betzel et al., 2016). Another reason is that methods like dFC and CAPs are based on k-means clustering which needs the number of clusters to

be predefined (Chen et al., 2017) and is inable to embed the the sequential transitions between brain states into the model (Chen et al., 2016). Judging from these concerns, the metastability underlying the adult lifespan may be captured by a more appropriate approach.

Hidden markov model (HMM) (Rabiner et al., 1989) is one of the promising techniques (Solo et al., 2018) to address such issues. HMM assumes that brain activity could be decomposed into a number of hidden states, which could be inferred from the observed data (i.e fMRI time-series). The transition probability between the hidden states and the fractional occupancy (FO, similar with the concept of dwell time, but is characterized in terms of probability) (Baker et al., 2014), are often used to quantify the temporal dynamics of the inferred hidden states. HMM has been applied to neuroimaging studies of multiple modalities such as EEG (Hunyadi et al., 2019; Stevner et al., 2019), MEG (Baker et al., 2014; Vidaurre et al., 2016; Quinn et al., 2018) and fMRI (Ryali et al., 2016; Vidaurre et al., 2017; Vidaurre et al., 2018; Taghia et al., 2018; Kottaram et al., 2019). HMM is the most effective when sample size is large due to the expanded feature space inherent in the probabilistic model (Chen et al., 2017), and is sufficient to capture quasi-stationary states of activity that are consistently recurring over a population (Baker et al., 2014). The capacity of HMM in discovering the switching dynamics in developmental maturation (Ryali et al., 2016), schizophrenia (Kottaram et al., 2019), multiple sclerosis (Van Schependom et al., 2019) and non-REM sleep (Stevner et al., 2019) proved that HMM is sufficient for characterizing the dynamic pattern of spontaneous brain activity across the adult lifespan.

In this study, we utilized HMM to estimate subject-specific FO and transition probabilities of discrete hidden states from rs-fMRI data, and investigated the relationship between these properties and age within a large sample cohort (n > 400, aged 19-80 years). Previous studies had revealed the age-difference in the functional interactions between default mode and control networks (Turner et al., 2015; Keller et

al., 2015; Spreng et al., 2017). Therefore, we aimed to find significant age-related correlation of FO and transition probability in states associated with these networks. Moreover, according to the expectation of Naik et al., (2017), we expected to find the state with lower transition probability and/or higher dwell time in the old cohort.

2. Materials and Methods

2.1 Participants and image acquisition

Data used in this study was selected from Southwest University adult lifespan dataset (http://fcon_1000.projects.nitrc.org/indi/retro/sald.html) (Wei et al., 2018). This dataset included 494 healthy subjects, none of which had a history of psychiatric or neurological disorders. Additionally, subjects who didn't satisfy the following criteria were excluded: 1) data loss, 2) excessive head motions (max head motion > 2.0 mm or 2.0 degree or mean framewise displacement (FD) > 0.2 mm), 3) extremely poor data quality (which cannot be successfully normalized). As a result, 422 subjects were included in this study (aged 19-80; mean age = 44.10; SD = 17.25; 166 males). The dataset collection was approved by the Research Ethics Committee of the Brain Imaging Center of Southwest University.

All of the data were collected at the Southwest University Center for Brain Imaging using a 3.0 T Siemens Trio MRI scanner. Each participant took part in 3D structural MRI and resting-state fMRI scans. For functional data, a 8-min scan of 242 contiguous whole-brain resting-state functional images was obtained using a gradient echo echo-planar-imaging (GRE-EPI) sequence with the following parameters: 32 axial slices, repetition time (TR)/echo time (TE) = 2000/30 ms, flip angle = 90 degrees, field of view (FOV) = 220 x 220 mm^2, thickness/slice gap = 3/1 mm, resolution matrix = 64 × 64. During the rs-fMRI scan, the subjects were instructed to lie quietly, close their eyes, and rest without thinking about any specific things but to refrain from falling asleep. For the structural data, a magnetization-prepared rapid gradient echo (MPRAGE) sequence was used to acquire high-resolution T1-weighted anatomical images (repetition time = 1,900 ms, echo time = 2.52 ms, inversion time = 900 ms, flip angle = 9 degrees, resolution matrix = 256 × 256, 176 sagittal slices,

thickness = 1 mm, FOV = 256 × 256 mm^2).

2.2.Image preprocessing

The data were preprocessed using data processing assistant for resting-state fMRI (DPARSF, http://rfmri.org/DPARSF) (Yan et al., 2016) with the following steps: removing the first 10 time points of each subject, slice timing correction, realignment to the mean functional volume to correct for head motion, nuisance regression including 24 motion parameters (Friston et al., 1996), linear trend and signals from white matter and cerebrospinal fluid, normalized to Montreal Neurological Institute space using the EPI template (Calhoun et al., 2017), smoothing (FWHM = 4 mm) and bandpass filtering (0.01 - 0.10 Hz).

2.3 Definition of functional networks

Our definition of resting-state networks (RSNs) was based on reference maps of 17 networks supported by Yeo and his colleagues (Yeo et al., 2011). The network names were consistent with Betzel et al. (2014) and were shown in Fig.1. For each subject, the averaged time course within each of the 17 RSNs were extracted from Yeo's template and then normalized separately (zero mean and unit standard deviation). The normalized time courses were temporally concatenated across all subjects, resulting in a two-dimensional matrix (networks × (time points × subjects)) to be input into HMM.

2.4 Hidden markov model

A brief flowchart of our approach was shown in Fig.2. HMM assumes that brain activity (observation sequence), is generated by a number of hidden states (state sequence) that are considered to be random variables following a Markov chain. The Markov chain could be fully determined by a set of basic parameters including initial probability distributions and the transition probability matrix of the hidden state variables. In a homogeneous Markov chain, probabilities of the current states only depend on those at the previous time point and the transition probability matrix (i.e. probabilities of states transiting from the previous to the current time point). The

observation matrix stands for the conditional probabilities of the observed data on hidden states, and has the distribution of multivariate Gaussian with the mean μ and covariance matrix Σ.

In this study, the HMM parameters were estimated by the HMM-MAR toolbox (https://github.com/OHBA-analysis/HMM-MAR) (Vidaurre et al., 2016; Vidaurre et al., 2017) using improved variational Bayes inference (Rezek and Robert, 2005), a popular inference paradigm that assumes certain simplifications in the HMM model (Jordan et al., 1998; Jaakkola et al., 2000). In this approach, traditional maximum-likelihood estimators are improved and replaced by *free energy*, which includes Kullback-Leibler divergence between the real and the factorised distribution and the entropy of the factorised distribution (Vidaurre et al., 2018). Therefore, parameters of HMM could be derived by minimization of the free energy. In this study, we ran HMM for 400 cycles with different initialization and chose the cycle with lowest free energy. Previous studies using HMM suggested that 8-12 states were suitable to get physiologically reasonable as well as replicable findings (Baker et al., 2014; Vidaurre et al., 2017; Vidaurre et al., 2018; Kottaram et al., 2019). Here, we choose K = 12 as number of states in accordance with Vidaurre et al., 2017 and Kottaram et al., 2019.

By applying variational Bayes inference on the entire data, we firstly estimated the group-level transition probability, the posterior probability of each state at each time points (or state time courses), the mean activation (μ, a 17 x 1 vector) and the covariance matrix (Σ, 17 x 17). The mean activation of sub-networks were firstly averaged for each network, and then were deemed as three levels according to the following criteria, (1) if the result was larger than 0.25, then the mean activation of this network was defined as ‘high’, (2) if the result was smaller than -0.25, then the mean activation of this network was defined as ‘low’ and (3) if the result was between -0.25 and 0.25, then the mean activation level of this network was defined as ‘moderate’.

In addition, due to our interest in subject-specific patterns of brain dynamics, subject-specific state variables were then calculated by making use of state time courses for each subject (Van schependom et al., 2019). These variables included subject-specific fractional occupancy (FO) and transition probability. Subject-specific FO was defined as the temporally averaged posterior probability of state k in one scan, which denoted the proportion of time spent visiting each state (Vidaurre et al., 2017).

2.5 Multiple linear regression

We employed a general linear model (GLM) to investigate the relationships between HMM parameters (subject-specific FO or transition probability) and age while taking the confounding effect of mean framewise displacement (FD) and sex into consideration. The effect of age was estimated by the t values of the corresponding regressors. Bon-ferroni correction was applied to correct for multiple comparisons. Subsequently, the adjusted FO (or transition probability) were obtained by removing contributions of mean FD and sex and were further plotted against age. The quadratic fit was applied to the scatter plots of adjusted FO (or transition probability) and age to illustrate the lifespan trajectories of FO (or transition probability).

3.Results

3.1 Mean activation patterns of the hidden brain states

Mean activation of the 12 hidden states were illustrated in Fig.3. Generally, there were no one-to-one mapping between these states and the typical RSNs. For example, for state 1, salience network (SN) and ventral attention network (VAN) showed high-level activation while DMN and limbic regions showed low-level activation. For state 2, DMN, somatomotor network (SMN) and limbic regions showed high-level activation while cognitive control (CCN), SN and VAN showed low-level activation. For state 7, both DMN and CCN showed high-level activation while SN and VAN showed low-level activation. For state 11, dorsal attention network (DAN) shows high-level activation while DMN and visual network shows low-level activation. For state 12, CCN showed high-level activation while SN, VAN and SMN showed low-level activation. In addition, state 3, 4, 5, 6 and 10 exhibited the similar patterns that almost

all networks showed high/low-level activation. Of particular interest, state 8 and 9 were two inactive states in that all RSNs showed moderate-level activation.

3.2 Relationships between FO and age

For states 1, 2 and 12, their FO exhibited significant decreases with age (Fig.4, $p < 0.05$, corrected). The FO of state 8 exhibited significant increase with age (Fig.4, $p < 0.05$, corrected), and showed a U-shaped lifespan trajectory with the valley around 32 years of age (Fig.5c), while the FO of states 1, 2 and 12 showed slow declines with age (Fig.5a, b, and d).

3.3 Relationships between transition probability and age

First, the transition probabilities from all states except 8 and 9 to state 8 showed significant increases with age while those from state 8 to states 1, 2, 5, 9 and 12 showed significant decreases with age (Fig.6, $p < 0.05$, corrected). Second, we found significant decreases for the transition probabilities from states 3 and 11 to state 2, and from state 7 to state 1 with age (Fig.6, $p < 0.05$, corrected). More interestingly, for the states 2 and 8, similar age-related patterns was found between their FOs and subject-specific transition probabilities. For example, the FO of state 8 increased with age, and the transition probabilities from the other states to state 8 increased with age as well.

Lifespan trajectories of some examples of adjusted transition probability are shown in Fig.7. Among them, the transition probabilities from state 7 to state 1 and from state 3 to state 2 decreased linearly with age (Fig.7a and b, $p < 0.05$, corrected). And the transition probabilities from state 11 to state 8 increased linearly with age (Fig.7e, $p < 0.05$, corrected). Besides, the transition probabilities from state 11 to state 2 and from state 8 to state 9 showed inverted U-shaped trajectories with age with peak ages at about 30 years (Fig.7c and f, $p < 0.05$, corrected), while the transition probabilities from state 7 to state 8 showed an U-shaped trajectory with age with peak ages at about 30 years (Fig.7d, $p < 0.05$, corrected).

4.Discussion

In the present study, we probed into the relationships between the metastability revealed by HMM and age using an relatively large sample adult-lifespan rs-fMRI dataset. Significant age-related changes of FO and transition probability were found in three hidden states involved in higher cognitive and default functions as well as one 'inactive' state. Our findings suggest that on one side, HMM methodology is effective in uncovering some intrinsic characteristics related to adult lifespan; On the other side, the human brain across the lifespan is accompanied with changes in the switching dynamics of spontaneous brain activity that may be critical for our better understanding about the normal development of the human brain functions.

4.1. Association between FO and age

Our results showed that the FO of states 1, 2 and 12 decreased linearly with age. State 1 is characterized by low-level activation of DMN and limbic regions, and high-level activation in SN-VAN. Similarly, state 2 is characterized by high-level activation of DMN, SMN and limbic regions, accompanied with low-level activation in CCN, SN and VAN. The observation that states 1 and 2 were visited less frequently in the elder might suggest weaken antagonistic relationships between DMN and SN-VAN, as well as DMN and CCN. Such antagonistic relationship likely reflects the 'anti-correlation' between task-negative network and task-positive networks. The result of state 2 was in agreement with the default-executive coupling hypothesis of aging (DECHA) model (Turner et al., 2015). Coupling between DMN and CCN were reported to be significantly higher in the elder (Turner et al., 2015; Keller et al., 2015; Spreng et al., 2017), and the enhanced coupling between these two networks indicated poorer autobiographical memory (Spreng et al., 2017) in old cohort .Additionally, the weaken antagonistic relationships between DMN and SN-VAN with the increase of age was in line with Tsvetanov et al. (2016) and Monteiro et al. (2019) that the functional connectivity between DMN and SN-VAN increased with age. Of note, there is conflict between our findings and two recent studies using sliding window approaches to explored the dynamic activity (Tian et al., 2018; Xia et al., 2019) where the dwell time of states characterized by positive coupling between DMN and CCN

(Tian et al., 2018; Xia et al., 2019) and between DMN and SN (Xia et al., 2019) were found to be inversely correlated with age. The discrepancy may be due to that the number of the brain states, obtained by k-means clustering, was so small (lower than 7) that one FC state may include more complicated spacial patterns than one HMM state.

Besides, state 12 denotes high-level activation in CCN and low-level activation in the other networks. The negative correlation between FO of this state with age may indicated that the decreased segregation or modularity of CCN in the elder. Numerous studies have found decreased segregation or modularity of functional networks in older adults (Cao et al., 2014; Chan et al., 2014; Betzel et al., 2014; Geerligs et al., 2014; Archer et al., 2016; King et al., 2018), and lower values of these measures were also associated with lower cognitive performance (Chan et al., 2014; King et al., 2018). More specifically, Betzel et al. (2014) and Monteiro et al., (2019) found that the decreased modularity/segregation of the control networks was significantly ($p < 0.05$, corrected) correlated with age, which were consistent with our results. This finding may cater to the dedifferentiation hypothesis that aging was associated with decreased specialization of functional networks (King et al., 2018).

Interestingly, the FO of state 8 was positively correlated with age, suggesting that the elder generally spent more time on this inactive state since all networks only showed moderate-level activity. Such inactive state was also found in Chen et al (2016) using HMM to explore the dynamical activity within healthy young adults (age: 22 - 36) and Kottaram et al., (2019) who applied HMM to explore the dynamical activity within the schizophrenia patient. Similarly, Tian et al. (2018) and Xia et al. (2019) employed the sliding window approach and also found that a state characterized by weak regional interaction throughout the brain was positively correlated the age. Chen et al., (2016) also found that most states often switch to this state and then transit back to other states from it. This state might reflect a transient 'ground state' (Chen et al., 2016) of the spontaneous brain activity.

Of note, the U-shaped lifespan trajectory of FO for the state 8 against age suggests the nonlinear relationship between the occurence of this state and age. The U-shaped lifespan trajectories were also observed for the mean between-network functional connectivity strength (Betzel et al., 2014), and the local and global efficiency in structural connectivity (Zhao et al., 2015) with similar valley around 30 years. Thus, our findings add further support to the view that non-linear trend might reveal the functional and structural turning point of adult lifespan. The quadratic decrease before 30 years might be highly related to maturation, and the quadratic increase after 30 years might be closely correlated with aging.

Similar with state 8, state 9 could be also considered as an 'inactive' state. However, it should be noted that there were a few subtle differences between them. First, the differences among the activity level of most networks were relatively modest in state 8, while the activity level of SN and VAN were relatively higher than other networks in state 9. Second, DMN and CCN showed negative activity in state 8, whereas almost all networks showed positive activity in state 9. Such differences imply that

they may represent different functional states of the resting brain and may explain the reasons why the FO of state 9 did not show significant decrease with age, nor age-related transitions as found in state 8.

4.2. Association between state transition probability and age

Another intriguing finding is that there was a tight correspondence between FO and transition probability of several hidden states. This was more obvious for the state 8. The elder had greater FO in state 8 than the younger people, generally accompanied by higher transition probabilities from other states to state 8 and lower transition probabilities from state 8 to other states. Although the causal relationship was unknown, the observed larger FO in the elder may be probably caused by the greater tendency of the spontaneous activity to enter the state 8 from the other states, and less tendency to leave state 8 for the other states. In that case, strong agreement was found between these two findings and the expectations of 'lower transition probability and/or higher dwell-time in a particular network state' by Naik et al., (2017).

Age-related transitions from state 11 to state 2 could account for the dynamic changes associated with aging. Our result indicated that the transition from the state with lower DMN.activity (i.e. state 11) to a state with higher DMN activity (i.e. state 2) become more difficult with the increase of age, which may explain why the elder spent less time in state 2, as reflected by their lower FO in state 2. This was in concordance with some stationary RSFC studies where they found the intra-connectivity of DMN

decreased with age (Andrews-Hanna et al., 2007; Mevel et al., 2013; Betzel et al., 2014; King et al., 2018). Likewise, age related asssociation of transition probability from state 3 to state 2 suggested that the transition from a state with higher activity of control network (i.e. state 3) to the state with lower activity of control network (i.e. state 2) become more difficult with the increase of age, which may explain why the elder spent less time in state 2, as reflected by their lower FO in state 2. And this finding is consistent with some stationary RSFC studies where they found the intra-connectivity of control network decreased with age (Betzel et al., 2014; Geerligs et al., 2014). Nevertheless, the decreased transition probability from state 7 to state 1 with age seems conflict with our interpretations about the results of state 2 since they exhibited an antagonistic relationship. The difficulty might be owing to our quite limited understanding about the brain dynamics per se as well as how it changes across the life span, which may be rather complex than expected. The development of dynamic analysis approaches including HMM is just at the starting point. Much future work is needed to investigate the neural mechanism underlying the activation patterns of, and the transitions among HMM state

Limitations

Several limitations should be taken into consideration. Firstly, it is worth mentioning that head motion can affect measures of functional connectivity (Power et al., 2012; Van Dijk et al., 2012), especially dynamic FC (Laumann et al., 2016). And functional imaging studies across development can suffer from age-related head motion and physiological noise (Power et al., 2012; Lehmann, White, Henson, & Geerligs, 2017). For this study, head motion may introduce false-positive age-related changes of FO and transition probability, though our strategies have included removing subjects with excessive mean FD, using 24 regression model in preprocessing step and selecting mean FD and age as covariables in multiple linear regression analysis. Secondly, imbalance of sex ratio in SALD dataset may induce gender effect. Although we only found significant sex-related change of state 7 ($p < 0.05$, corrected) in multiple linear regression analysis, the replicability of our study may be difficult due to the lack of

sufficient male participants. The ongoing HCP-A (Human Connectome project in aging) project could be capable of tackling this issue in the future (Bookheimer et al., 2019). Thirdly, we estimated HMM parameters using concatenating data from all individuals, and thus every subject shared a common set of states, which was not suitable to capture subject-specific traits and make personalized diagnosis on disease. Future studies are expected to improve the specificity of this approach. Lastly, 400 training cycles of different initialization could not guarantee the global optimum solution, methods like simulated annealing (Lee et al., 2010) or genetic algorithm (Won et al., 2004) may applied to this model and solve this problem.

Conclusions

This study sharpened our understanding of the link between resting brain dynamics and adult lifespan. We found the elder were probable to spend more time on a state with moderate-level activation of all networks, and less time on states showing antagonistic activity between pairs of networks including DMN, control and SalVentAttn. In addition, the transition probabilities between certain pair of states also showed age-related changes, indicating the age-related regulation of default mode and control network. Moreover, these age-related FO changes may be due to the transitions among the corresponding hidden states. Therefore, HMM is a huge potential tool for discovering the dynamic alteration across adult lifespan.

References

Allen EA, Damaraju E, Plis SM, Erhardt EB, Eichele T, Calhoun VD. 2014. Tracking whole-brain connectivity dynamics in the resting state. Cereb Cortex. 24:663-676.

Andrews-Hanna JR, Snyder AZ, Vincent JL, Lustig C, Head D, Raichle ME, Buckner RL. 2007. Disruption of large-scale brain systems in advanced aging. Neuron. 56:924-935.

Baker AP, Brookes MJ, Rezek IA, Smith SM, Behrens T, Probert Smith PJ, Woolrich M. 2014. Fast transient networks in spontaneous human brain activity. Elife. 3:e01867.

Betzel RF, Byrge L, He Y, Goni J, Zuo XN, Sporns O. 2014. Changes in structural and functional connectivity among resting-state networks across the human lifespan. Neuroimage. 102 Pt 2:345-357.

Betzel RF, Fukushima M, He Y, Zuo XN, Sporns O. 2016. Dynamic fluctuations coincide with periods of high and low modularity in resting-state functional brain networks. Neuroimage. 127:287-297.

Bookheimer SY, Salat DH, Terpstra M, Ances BM, Barch DM, Buckner RL, Burgess GC, Curtiss SW, Diaz-Santos M, Elam JS, Fischl B, Greve DN, Hagy HA, Harms MP, Hatch OM, Hedden T, Hodge C, Japardi KC, Kuhn TP, Ly TK, Smith SM, Somerville LH, Ugurbil K, van der Kouwe A, Van Essen D, Woods RP, Yacoub E. 2019. The Lifespan Human Connectome Project in Aging: An overview. Neuroimage. 185:335-348.

Calhoun VD, Wager TD, Krishnan A, Rosch KS, Seymour KE, Nebel MB, Mostofsky SH, Nyalakanai P, Kiehl K. 2017. The impact of T1 versus EPI spatial normalization templates for fMRI data analyses. Hum Brain Mapp. 38:5331-5342.

Cao M, Wang JH, Dai ZJ, Cao XY, Jiang LL, Fan FM, Song XW, Xia MR, Shu N, Dong Q, Milham MP, Castellanos FX, Zuo XN, He Y. 2014. Topological organization of the human brain functional connectome across the lifespan. Dev Cogn Neurosci. 7:76-93.

Chan MY, Park DC, Savalia NK, Petersen SE, Wig GS. 2014. Decreased segregation of brain systems across the healthy adult lifespan. Proc Natl Acad Sci U S A. 111:E4997-5006.

Chen JE, Rubinov M, Chang C. 2017. Methods and Considerations for Dynamic Analysis of Functional MR Imaging Data. Neuroimaging Clin N Am. 27:547-560.

Chen S, Langley J, Chen X, Hu X. 2016. Spatiotemporal Modeling of Brain Dynamics Using Resting-State Functional Magnetic Resonance Imaging with Gaussian Hidden Markov Model. Brain Connect. 6:326-334.

Chen Y, Liu YN, Zhou P, Zhang X, Wu Q, Zhao X, Ming D. 2018. The Transitions Between Dynamic Micro-States Reveal Age-Related Functional Network Reorganization. Front Physiol. 9:1852.

Damaraju E, Allen EA, Belger A, Ford JM, McEwen S, Mathalon DH, Mueller BA, Pearlson GD, Potkin SG, Preda A, Turner JA, Vaidya JG, van Erp TG, Calhoun VD. 2014. Dynamic functional connectivity analysis reveals transient states of dysconnectivity in schizophrenia. Neuroimage Clin. 5:298-308.

de Vos F, Koini M, Schouten TM, Seiler S, van der Grond J, Lechner A, Schmidt R, de Rooij M, Rombouts S. 2018. A comprehensive analysis of resting state fMRI measures to classify individual patients with Alzheimer's disease. Neuroimage. 167:62-72.

Diez-Cirarda M, Strafella AP, Kim J, Pena J, Ojeda N, Cabrera-Zubizarreta A, Ibarretxe-Bilbao N. 2018. Dynamic functional connectivity in Parkinson's disease patients with mild cognitive impairment and normal cognition. Neuroimage Clin. 17:847-855.

Finotelli P, Dipasquale O, Costantini I, Pini A, Baglio F, Baselli G, Dulio P, Cercignani M. 2018. Exploring resting-state functional connectivity invariants across the lifespan in healthy people by means of a recently proposed graph theoretical model. PLoS One. 13:e0206567.

Fox MD, Snyder AZ, Vincent JL, Corbetta M, Van Essen DC, Raichle ME. 2005. The human brain is intrinsically organized into dynamic, anticorrelated functional networks. Proc Natl Acad Sci U S A. 102:9673-9678.

Friston KJ, Williams S, Howard R, Frackowiak RS, Turner R. 1996. Movement-related effects in fMRI time-series. Magn Reson Med. 35:346-355.

Fu Z, Caprihan A, Chen J, Du Y, Adair JC, Sui J, Rosenberg GA, Calhoun VD. 2019. Altered static and dynamic functional network connectivity in Alzheimer's disease and subcortical ischemic vascular disease: shared and specific brain connectivity abnormalities. Hum Brain Mapp. 40:3203-3221.

Grady CL, Springer MV, Hongwanishkul D, McIntosh AR, Winocur G. 2006. Age-related changes in brain activity across the adult lifespan. J Cogn Neurosci. 18:227-241.

Greicius MD, Krasnow B, Reiss AL, Menon V. 2003. Functional connectivity in the resting brain: a network analysis of the default mode hypothesis. Proc Natl Acad Sci U S A. 100:253-258.

Hindriks R, Adhikari MH, Murayama Y, Ganzetti M, Mantini D, Logothetis NK, Deco G. 2016. Can sliding-window correlations reveal dynamic functional connectivity in resting-state fMRI? Neuroimage. 127:242-256.
Hunyadi B, Woolrich MW, Quinn AJ, Vidaurre D, De Vos M. 2019. A dynamic system of brain networks revealed by fast transient EEG fluctuations and their fMRI correlates. Neuroimage. 185:72-82.
Jaakkola TS. Tutorial on Variational Approximation Methods. 2000. Advanced Mean Field Methods: Theory and Practice. MIT Press
Jordan MI, Ghahramani Z, Jaakkola TS, and Saul LK. 2019. An Introduction to Variational Methods for Graphical Models. In M.I. Jordan, editor, Learning in Graphical Models. Kluwer Academic Press
Keller JB, Hedden T, Thompson TW, Anteraper SA, Gabrieli JD, Whitfield-Gabrieli S. 2015. Resting-state anticorrelations between medial and lateral prefrontal cortex: association with working memory, aging, and individual differences. Cortex. 64:271-280.
Kennedy KM, Boylan MA, Rieck JR, Foster CM, Rodrigue KM. 2017. Dynamic range in BOLD modulation: lifespan aging trajectories and association with performance. Neurobiol Aging. 60:153-163.
Kim J, Criaud M, Cho SS, Diez-Cirarda M, Mihaescu A, Coakeley S, Ghadery C, Valli M, Jacobs MF, Houle S, Strafella AP. 2017. Abnormal intrinsic brain functional network dynamics in Parkinson's disease. Brain. 140:2955-2967.
King BR, van Ruitenbeek P, Leunissen I, Cuypers K, Heise KF, Santos Monteiro T, Hermans L, Levin O, Albouy G, Mantini D, Swinnen SP. 2018. Age-Related Declines in Motor Performance are Associated With Decreased Segregation of Large-Scale Resting State Brain Networks. Cereb Cortex. 28:4390-4402.
Kottaram A, Johnston LA, Cocchi L, Ganella EP, Everall I, Pantelis C, Kotagiri R, Zalesky A. 2019. Brain network dynamics in schizophrenia: Reduced dynamism of the default mode network. Hum Brain Mapp. 40:2212-2228.
Laumann TO, Snyder AZ, Mitra A, Gordon EM, Gratton C, Adeyemo B, Gilmore AW, Nelson SM, Berg JJ, Greene DJ, McCarthy JE, Tagliazucchi E, Laufs H, Schlaggar

BL, Dosenbach NUF, Petersen SE. 2017. On the Stability of BOLD fMRI Correlations. Cereb Cortex. 27:4719-4732.
Lee JS, Park CH. 2010. Hybrid simulated annealing and its application to optimization of hidden Markov models for visual speech recognition. IEEE Trans Syst Man Cybern B Cybern. 40:1188-1196.
Lehmann BCL, White SR, Henson RN, Cam C, Geerligs L. 2017. Assessing dynamic functional connectivity in heterogeneous samples. Neuroimage. 157:635-647.
Leonardi N, Van De Ville D. 2015. On spurious and real fluctuations of dynamic functional connectivity during rest. Neuroimage. 104:430-436.
Liu X, Duyn JH. 2013. Time-varying functional network information extracted from brief instances of spontaneous brain activity. Proc Natl Acad Sci U S A. 110:4392-4397.
Monteiro TS, King BR, Zivari Adab H, Mantini D, Swinnen SP. 2019. Age-related differences in network flexibility and segregation at rest and during motor performance. Neuroimage. 194:93-104.
Naik S, Banerjee A, Bapi RS, Deco G, Roy D. 2017. Metastability in Senescence. Trends Cogn Sci. 21:509-521.
Narvacan K, Treit S, Camicioli R, Martin W, Beaulieu C. 2017. Evolution of deep gray matter volume across the human lifespan. Hum Brain Mapp. 38:3771-3790.
Power JD, Barnes KA, Snyder AZ, Schlaggar BL, Petersen SE. 2012. Spurious but systematic correlations in functional connectivity MRI networks arise from subject motion. Neuroimage. 59:2142-2154.
Putcha D, Ross RS, Cronin-Golomb A, Janes AC, Stern CE. 2016. Salience and Default Mode Network Coupling Predicts Cognition in Aging and Parkinson's Disease. J Int Neuropsychol Soc. 22:205-215.
Quinn AJ, Vidaurre D, Abeysuriya R, Becker R, Nobre AC, Woolrich MW. 2018. Task-Evoked Dynamic Network Analysis Through Hidden Markov Modeling. Front Neurosci. 12:603.
Rabany L, Brocke S, Calhoun VD, Pittman B, Corbera S, Wexler BE, Bell MD, Pelphrey K, Pearlson GD, Assaf M. 2019. Dynamic functional connectivity in

schizophrenia and autism spectrum disorder: Convergence, divergence and classification. Neuroimage Clin. 24:101966.
Rabiner L.R. 1989. A Tutorial on Hidden Markov Models and Selected Applications in Speech Recognition. Proceeding of the IEEE, 77(2):257–284.
Rashid B, Damaraju E, Pearlson GD, Calhoun VD. 2014. Dynamic connectivity states estimated from resting fMRI Identify differences among Schizophrenia, bipolar disorder, and healthy control subjects. Front Hum Neurosci. 8:897.
Rezek I, Roberts S. 2005. Ensemble hidden markov models with extended observation densities for biosignal analysis. Probabilistic Modeling in Bioinformatics and Medical Informatics. pp. 419–450.
Riddle WR, DonLevy SC, Lee H. 2010. Modeling brain tissue volumes over the lifespan: quantitative analysis of postmortem weights and in vivo MR images. Magn Reson Imaging. 28:716-720.
Ryali S, Supekar K, Chen T, Kochalka J, Cai W, Nicholas J, Padmanabhan A, Menon V. 2016. Temporal Dynamics and Developmental Maturation of Salience, Default and Central-Executive Network Interactions Revealed by Variational Bayes Hidden Markov Modeling. PLoS Comput Biol. 12:e1005138.
Schumacher J, Peraza LR, Firbank M, Thomas AJ, Kaiser M, Gallagher P, O'Brien JT, Blamire AM, Taylor JP. 2019. Dynamic functional connectivity changes in dementia with Lewy bodies and Alzheimer's disease. Neuroimage Clin. 22:101812.
Solo V, Poline JB, Lindquist MA, Simpson SL, Bowman FD, Chung MK, Cassidy B. 2018. Connectivity in fMRI: Blind Spots and Breakthroughs. IEEE Trans Med Imaging. 37:1537-1550.
Spreng RN, Lockrow AW, DuPre E, Setton R, Spreng KAP, Turner GR. 2018. Semanticized autobiographical memory and the default - executive coupling hypothesis of aging. Neuropsychologia. 110:37-43.
Stevner ABA, Vidaurre D, Cabral J, Rapuano K, Nielsen SFV, Tagliazucchi E, Laufs H, Vuust P, Deco G, Woolrich MW, Van Someren E, Kringelbach ML. 2019. Discovery of key whole-brain transitions and dynamics during human wakefulness and non-REM sleep. Nat Commun. 10:1035.

Taghia J, Cai W, Ryali S, Kochalka J, Nicholas J, Chen T, Menon V. 2018. Uncovering hidden brain state dynamics that regulate performance and decision-making during cognition. Nat Commun. 9:2505.

Tian L, Li Q, Wang C, Yu J. 2018. Changes in dynamic functional connections with aging. Neuroimage. 172:31-39.

Tsvetanov KA, Henson RN, Tyler LK, Razi A, Geerligs L, Ham TE, Rowe JB, Cambridge Centre for A, Neuroscience. 2016. Extrinsic and Intrinsic Brain Network Connectivity Maintains Cognition across the Lifespan Despite Accelerated Decay of Regional Brain Activation. J Neurosci. 36:3115-3126.

Turner GR, Spreng RN. 2015. Prefrontal Engagement and Reduced Default Network Suppression Co-occur and Are Dynamically Coupled in Older Adults: The Default-Executive Coupling Hypothesis of Aging. J Cogn Neurosci. 27:2462-2476.

Van Dijk KR, Sabuncu MR, Buckner RL. 2012. The influence of head motion on intrinsic functional connectivity MRI. Neuroimage. 59:431-438.

Van Schependom J, Vidaurre D, Costers L, Sjogard M, D'Hooghe M B, D'Haeseleer M, Wens V, De Tiege X, Goldman S, Woolrich M, Nagels G. 2019. Altered transient brain dynamics in multiple sclerosis: Treatment or pathology? Hum Brain Mapp. 40:4789-4800.

Vannest J, Maloney T, Kay B, Siegel M, Allendorfer JB, Banks C, Altaye M, Szaflarski JP. 2015. Age related-changes in the neural basis of self-generation in verbal paired associate learning. Neuroimage Clin. 7:537-546.

Vidaurre D, Abeysuriya R, Becker R, Quinn AJ, Alfaro-Almagro F, Smith SM, Woolrich MW. 2018. Discovering dynamic brain networks from big data in rest and task. Neuroimage. 180:646-656.

Vidaurre D, Quinn AJ, Baker AP, Dupret D, Tejero-Cantero A, Woolrich MW. 2016. Spectrally resolved fast transient brain states in electrophysiological data. Neuroimage. 126:81-95.

Vidaurre D, Smith SM, Woolrich MW. 2017. Brain network dynamics are hierarchically organized in time. Proc Natl Acad Sci U S A. 114:12827-12832.

Wei D, Zhuang K, Ai L, Chen Q, Yang W, Liu W, Wang K, Sun J, Qiu J. 2018. Structural and functional brain scans from the cross-sectional Southwest University adult lifespan dataset. Sci Data. 5:180134.

Won KJ, Prugel-Bennett A, Krogh A. 2004. Training HMM structure with genetic algorithm for biological sequence analysis. Bioinformatics. 20:3613-3619.

Xia M, Wang J, He Y. 2013. BrainNet Viewer: a network visualization tool for human brain connectomics. PLoS One. 8:e68910.

Xia Y, Chen Q, Shi L, Li M, Gong W, Chen H, Qiu J. 2019. Tracking the dynamic functional connectivity structure of the human brain across the adult lifespan. Hum Brain Mapp. 40:717-728.

Yan CG, Wang XD, Zuo XN, Zang YF. 2016. DPABI: Data Processing & Analysis for (Resting-State) Brain Imaging. Neuroinformatics. 14:339-351.

Yang Z, Chang C, Xu T, Jiang L, Handwerker DA, Castellanos FX, Milham MP, Bandettini PA, Zuo XN. 2014. Connectivity trajectory across lifespan differentiates the precuneus from the default network. Neuroimage. 89:45-56.

Yeo BT, Krienen FM, Sepulcre J, Sabuncu MR, Lashkari D, Hollinshead M, Roffman JL, Smoller JW, Zollei L, Polimeni JR, Fischl B, Liu H, Buckner RL. 2011. The organization of the human cerebral cortex estimated by intrinsic functional connectivity. J Neurophysiol. 106:1125-1165.

Zhao T, Cao M, Niu H, Zuo XN, Evans A, He Y, Dong Q, Shu N. 2015. Age-related changes in the topological organization of the white matter structural connectome across the human lifespan. Hum Brain Mapp. 36:3777-3792.

Zhuang X, Walsh RR, Sreenivasan K, Yang Z, Mishra V, Cordes D. 2018. Incorporating spatial constraint in co-activation pattern analysis to explore the dynamics of resting-state networks: An application to Parkinson's disease. Neuroimage. 172:64-84.

Figure 1

Yeo's 17-network parcellation of human cerebral cortex. The parcellation are mapped on the smoothed ICBM 152 surface using BrainNet Viewer. Network names are identical with Betzel et al., (2014).

Figure 2

The brief flowchart of our approach. (a) Network-averaged fMRI timeseries were temporally concatenated and fed into HMM. (b) Hidden Markov model. S_t are random variables following a Markov chain, which denotes the hidden states in time point t. Similarly, Xt denotes the observed values from networks-averaged timeseries in time point t. The conditional probabilities of the observed data on hidden states have the distribution of multi-Gaussian with mean vectors μ and covariance matrices Σ . (c) Mean activation of states. Mean vectors μ are projected to the ICBM 152 surface using BrainNet toolbox. (d) Subject-specific transition probability matrix. Elements Aij denotes the transition probability $P(S_t | S_{t-1})$ from one state i to another state j. (e) State distribution of K = 12 states. The posterior probability of K states is estimated via variational Bayes inference, with each color representing a particular state. (f) Subject-specific fractional occupancy, which is defined as the temporally averaged posterior probability of state k in one scan. (g) Multiple linear regression analysis. Subject-specific FO and transition probability are modeled as explained variables, while age is modeled as a explanatory variable (mean framewise displacement and sex are modeled as covariables).

Figure 3

Mean activation of the 12 hidden states. Positive values were shown in warm color and negative values were shown in cool color. Positive values which is less than 0.01

and negative values which is more than -0.01 were filtered out.

Figure 4

Significant age-related changes of subjects' fractional occupancy. The value of each bar denotes the t value of age coefficient (β_1) of MLR model for FO and age (including mean FD and sex as covariables). Asterisks (*) denote $p < 0.05$ (Corrected).

Figure 5

Lifespan trajectories of subjects' fractional occupancy. Each asterisk (*) denotes the adjusted FO value of each subject. The red dot denotes the valley of the quadratic fitting curve. (a) Lifespan trajectories of the fractional occupancy of state 1. (b) Lifespan trajectories of the fractional occupancy of state 2. (c) Lifespan trajectories of the fractional occupancy of state 8. (d) Lifespan trajectories of the fractional occupancy of state 12.

Figure 6

Significant age-related changes of subjects' transition probabilities. Diagonal and non-significant ($p > 0.05$, corrected) elements were removed. Colorbar denotes the t value of age coefficient (β_1) of MLR model for transition probability and age (including mean FD and sex as covariables).

Figure 7

Lifespan trajectories of subjects' transition probability. Each asterisk (*) denotes the adjusted transition probability of each subject. The red dot denotes the peak/valley of the quadratic fitting curve.(a) Lifespan trajectories of the transition probability from

state 7 to state 1. (b) Lifespan trajectories of the transition probability from state 3 to state 2. (c) Lifespan trajectories of the transition probability from state 11 to state 2. (d) Lifespan trajectories of the transition probability from state 7 to state 8. (e) Lifespan trajectories of the transition probability from state 11 to state 8. (f) Lifespan trajectories of the transition probability from state 8 to state 9.

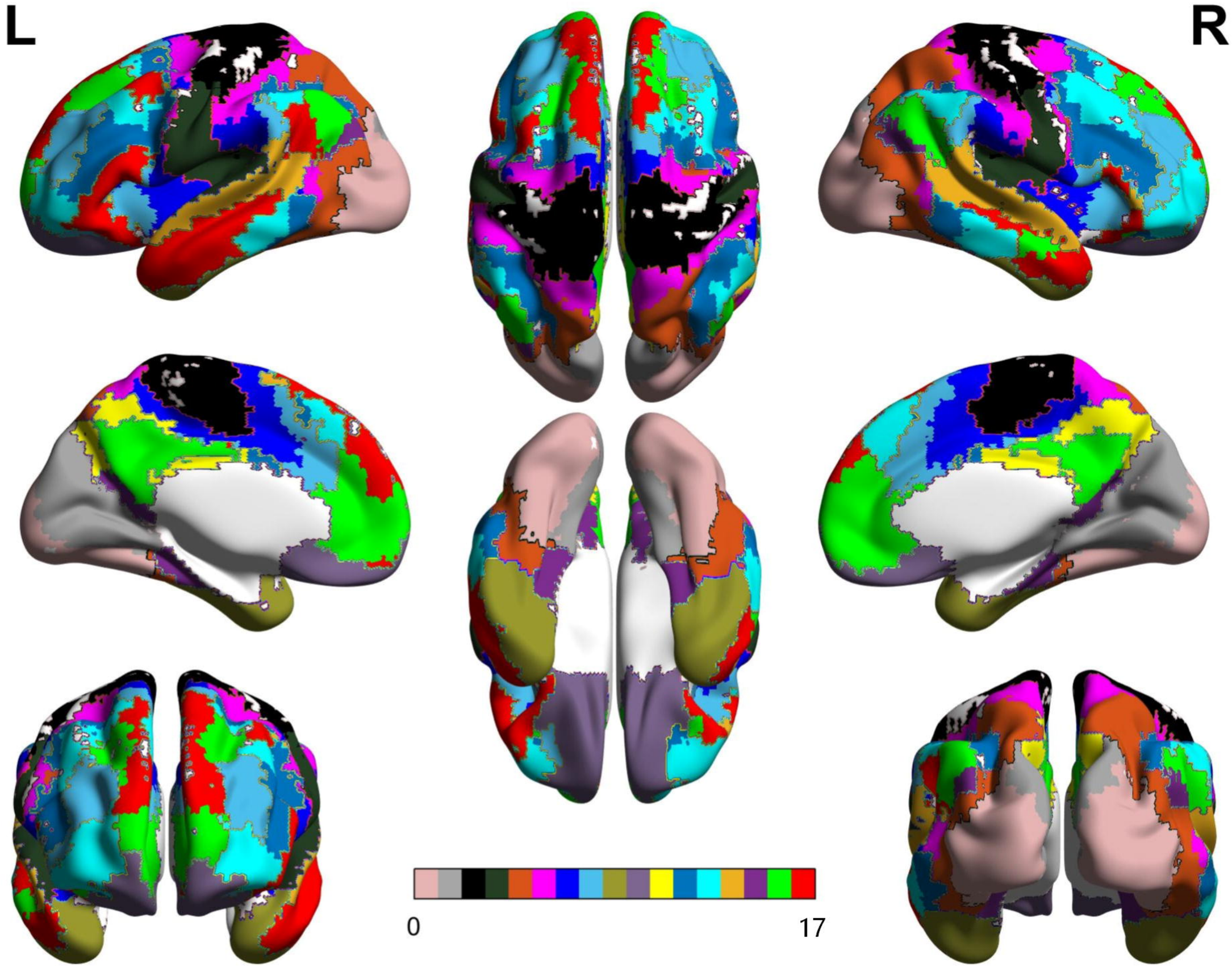

Network number and color	1	2		4	5	6	7	8	9	10	11	12	13	14	15	16	17
Network name	Visual peripheral	Visual central	Somatomotor A	Somatomotor B	Dorsal attention A	Dorsal attention B	Salience / Ventral attention A	Salience / Ventral attention B	Limbic A	Limbic B	Control C	Control A	Control B	Default D	Default C	Default A	Default B

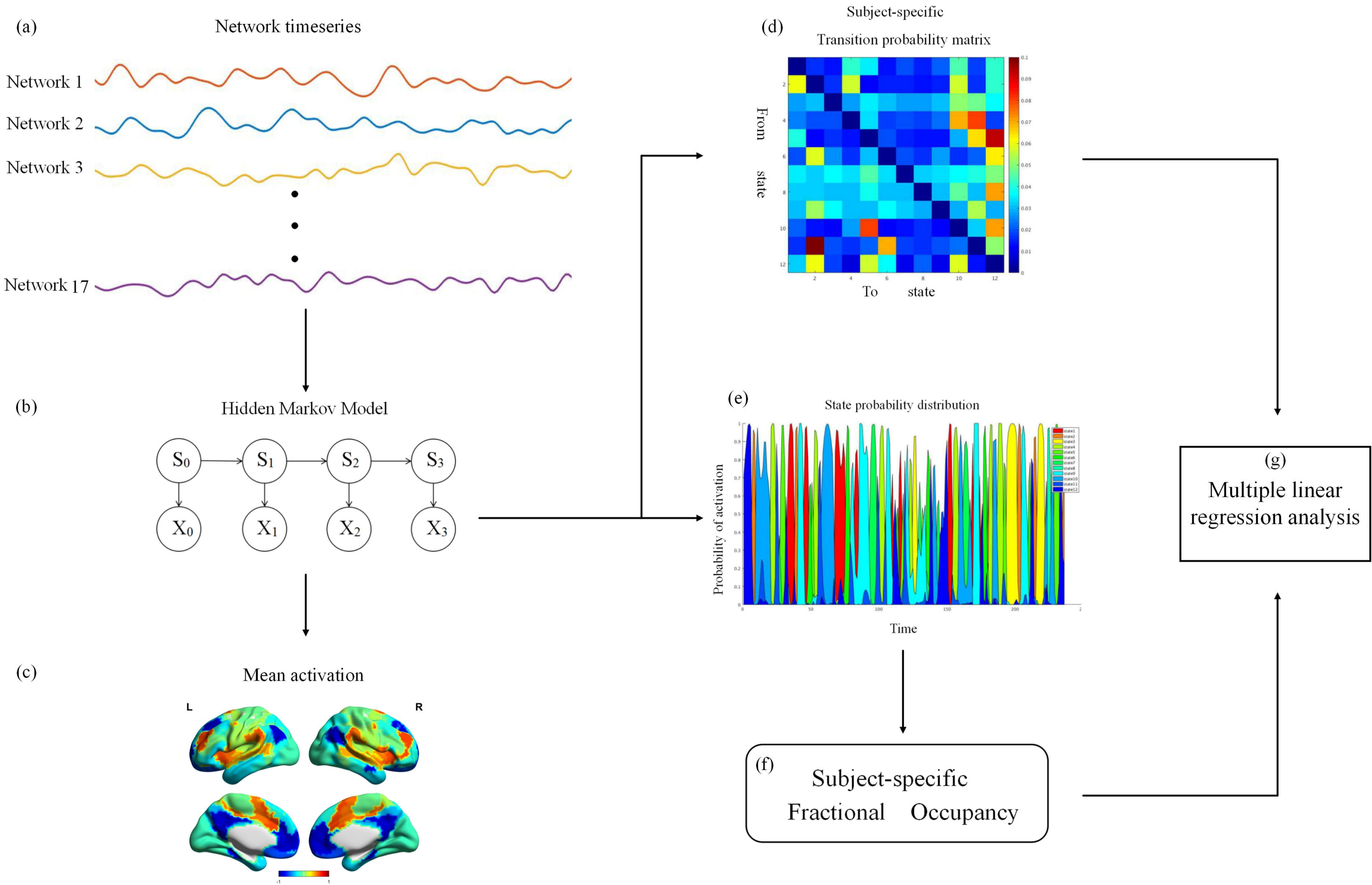
(a)
Network timeseries
Network 1
Network 2
Network 3
Network 17
(b)
Hidden Markov Model
S0
S1
S2
S3
X0
X1
X2
X3
(c)
Mean activation
L
R
(d)
Subject-specific
Transition probability matrix
From state
To state
(e)
State probability distribution
Probability of activation
Time
(f)
Subject-specific
Fractional Occupancy
(g)
Multiple linear
regression analysis

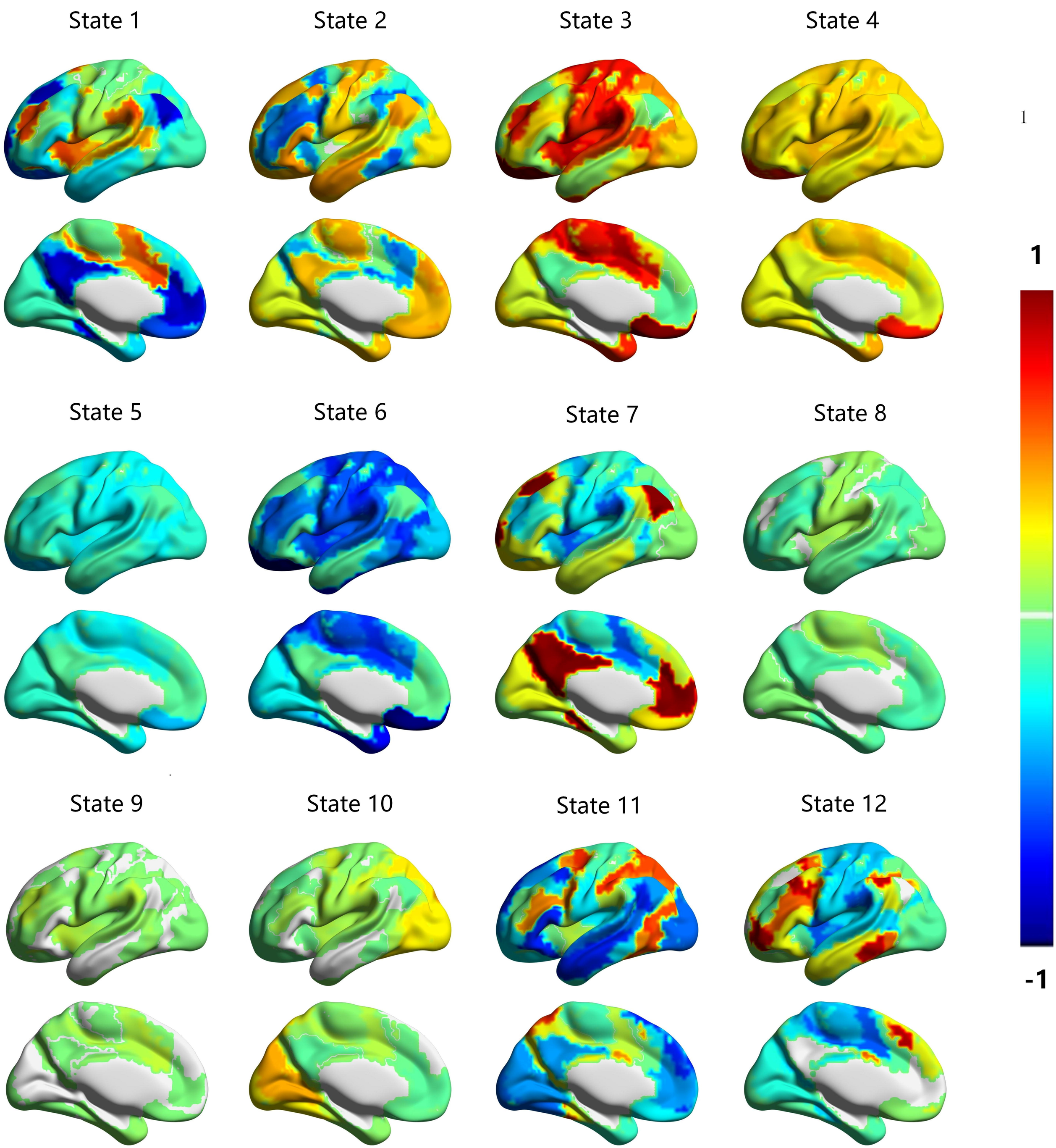
State 1
State 2
State 3
State 4
State 5
State 6
State 7
State 8
State 9
State 10
State 11
State 12
1
1
-1

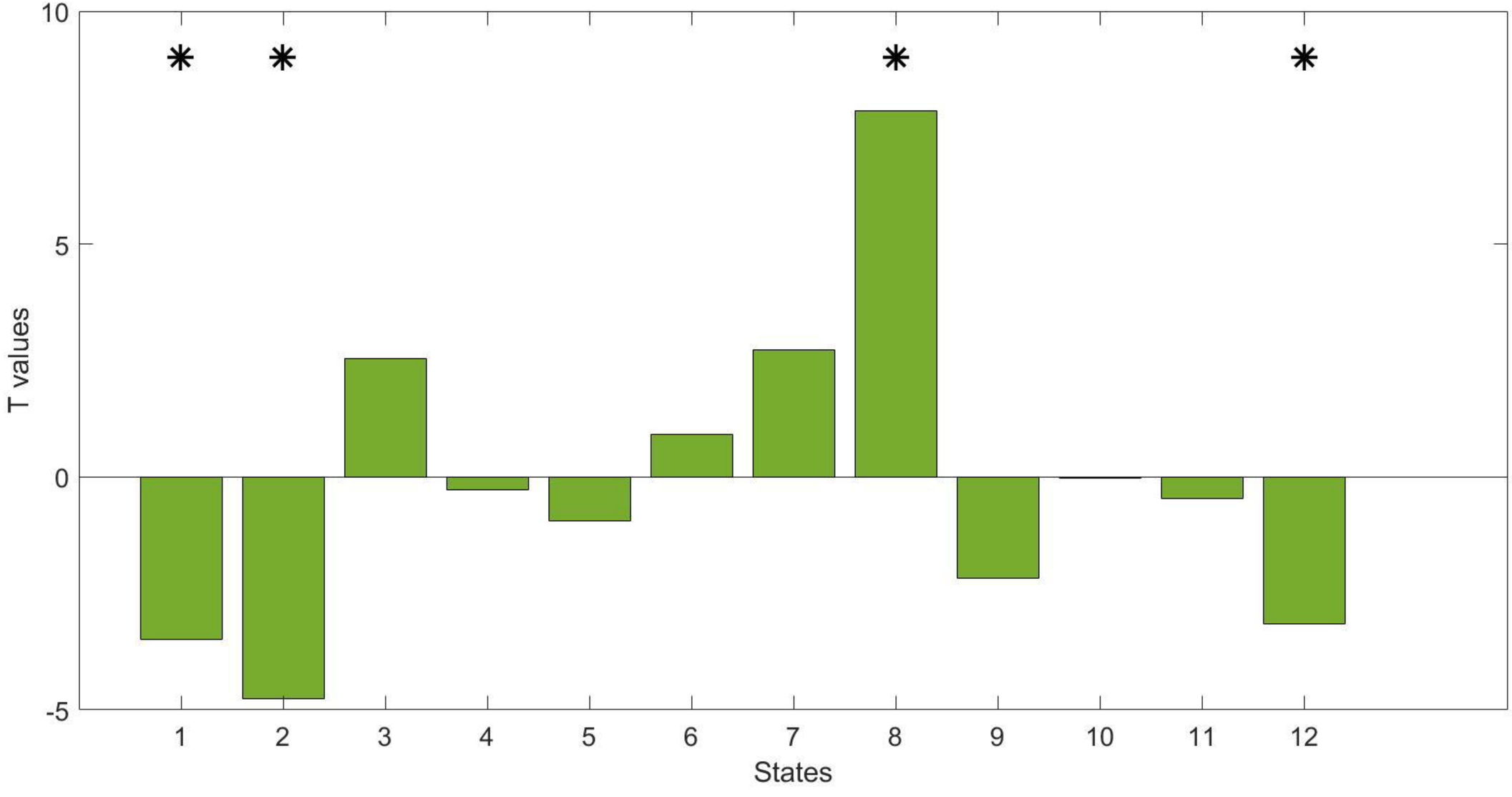
10
5
0
-5
T values
1
2
3
4
5
6
7
8
9
10
11
12
States

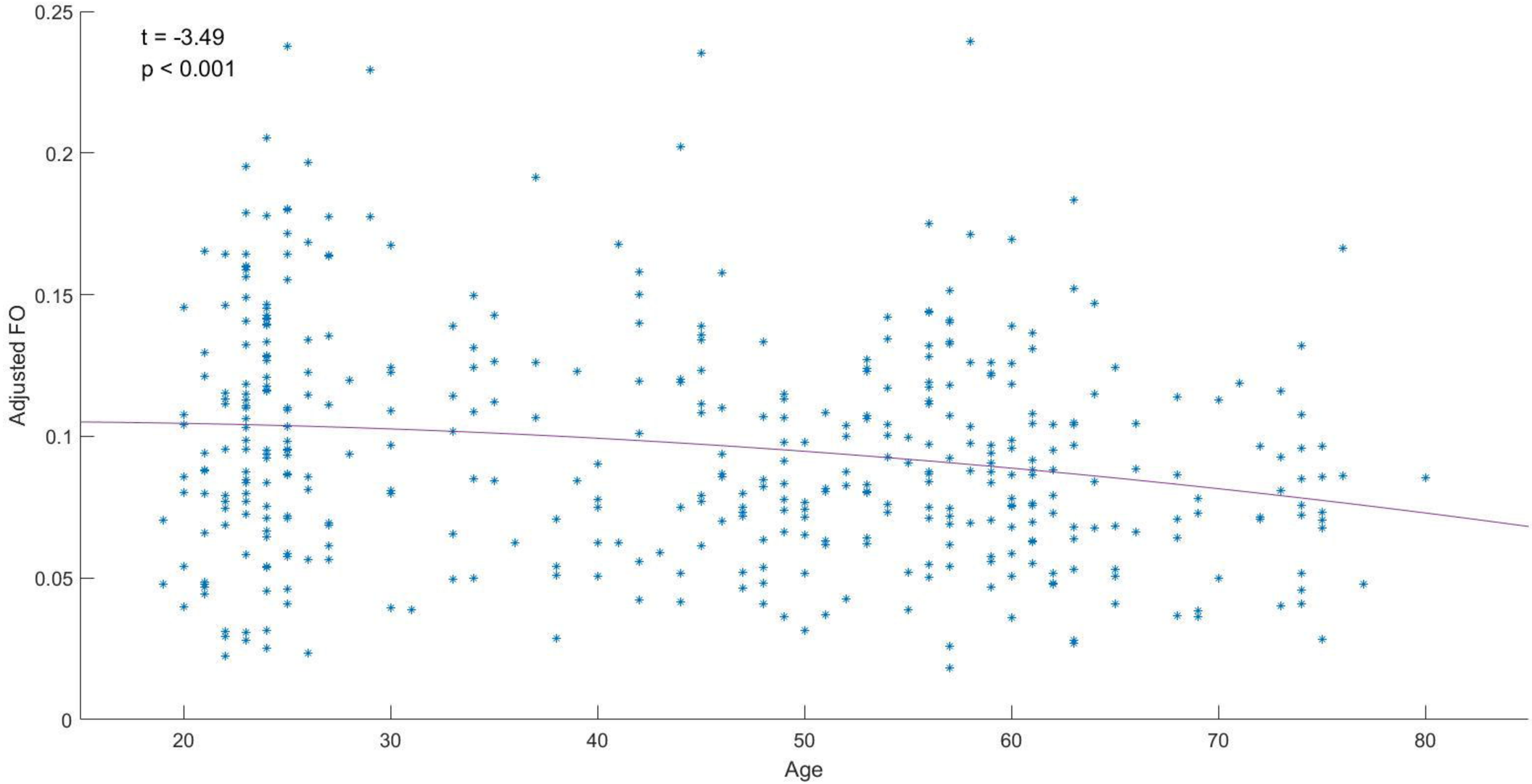
t = -3.49
p < 0.001
Adjusted FO
Age
0.25
0.2
0.15
0.1
0.05
0
20
30
40
50
60
70
80

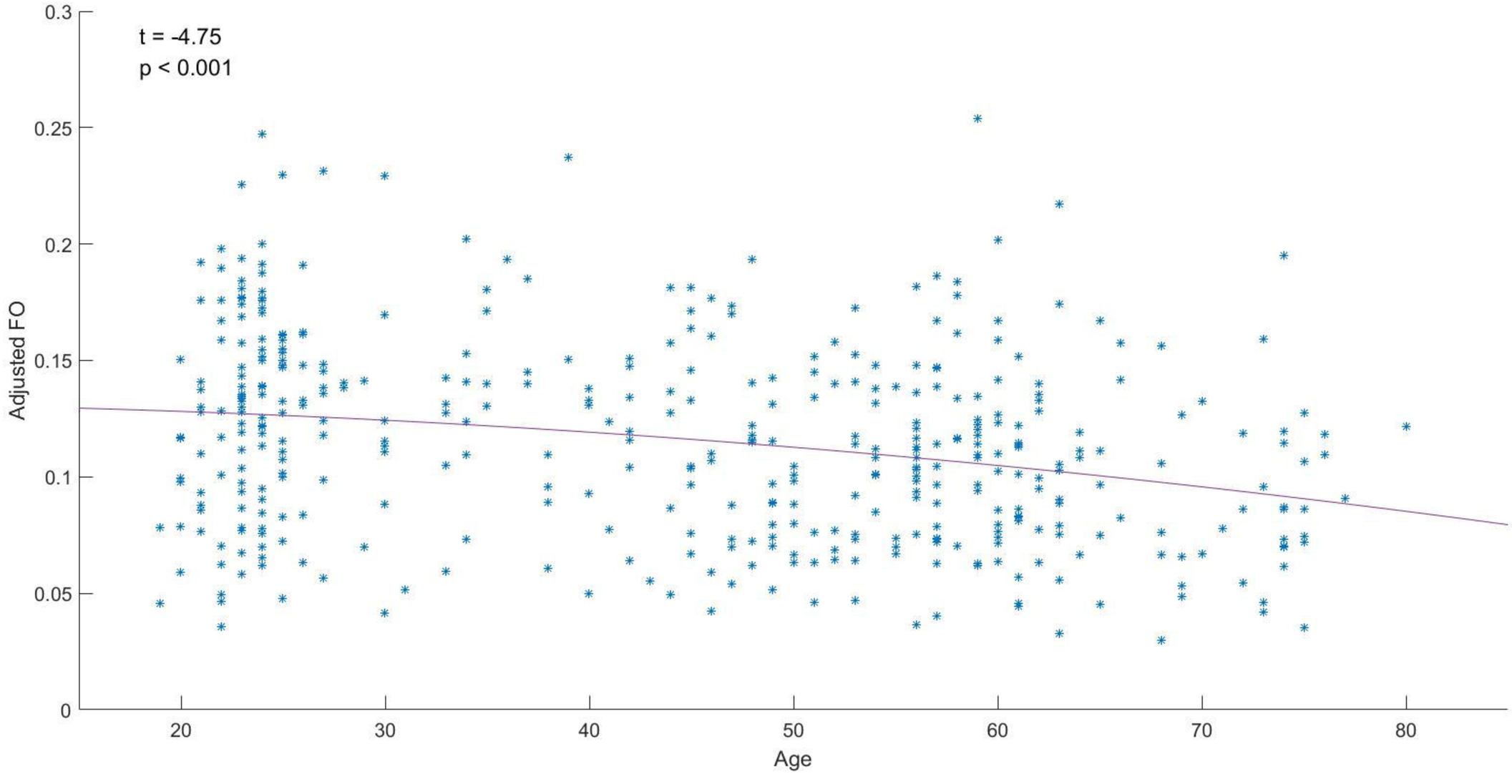
t = -4.75
p < 0.001
Adjusted FO
Age
0.3
0.25
0.2
0.15
0.1
0.05
0
20
30
40
50
60
70
80

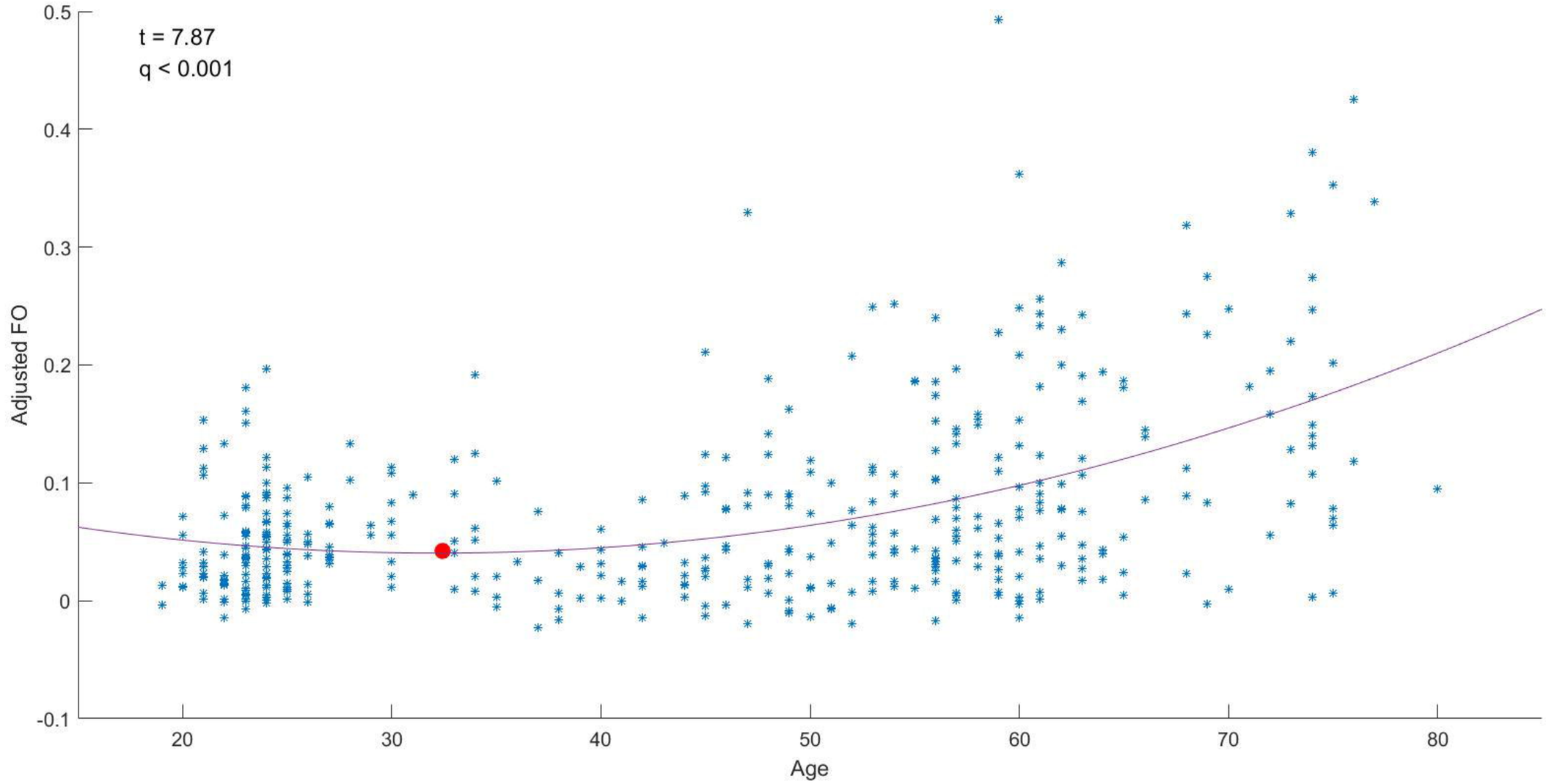
t = 7.87
q < 0.001
Adjusted FO
Age
0.5
0.4
0.3
0.2
0.1
0
-0.1
20
30
40
50
60
70
80

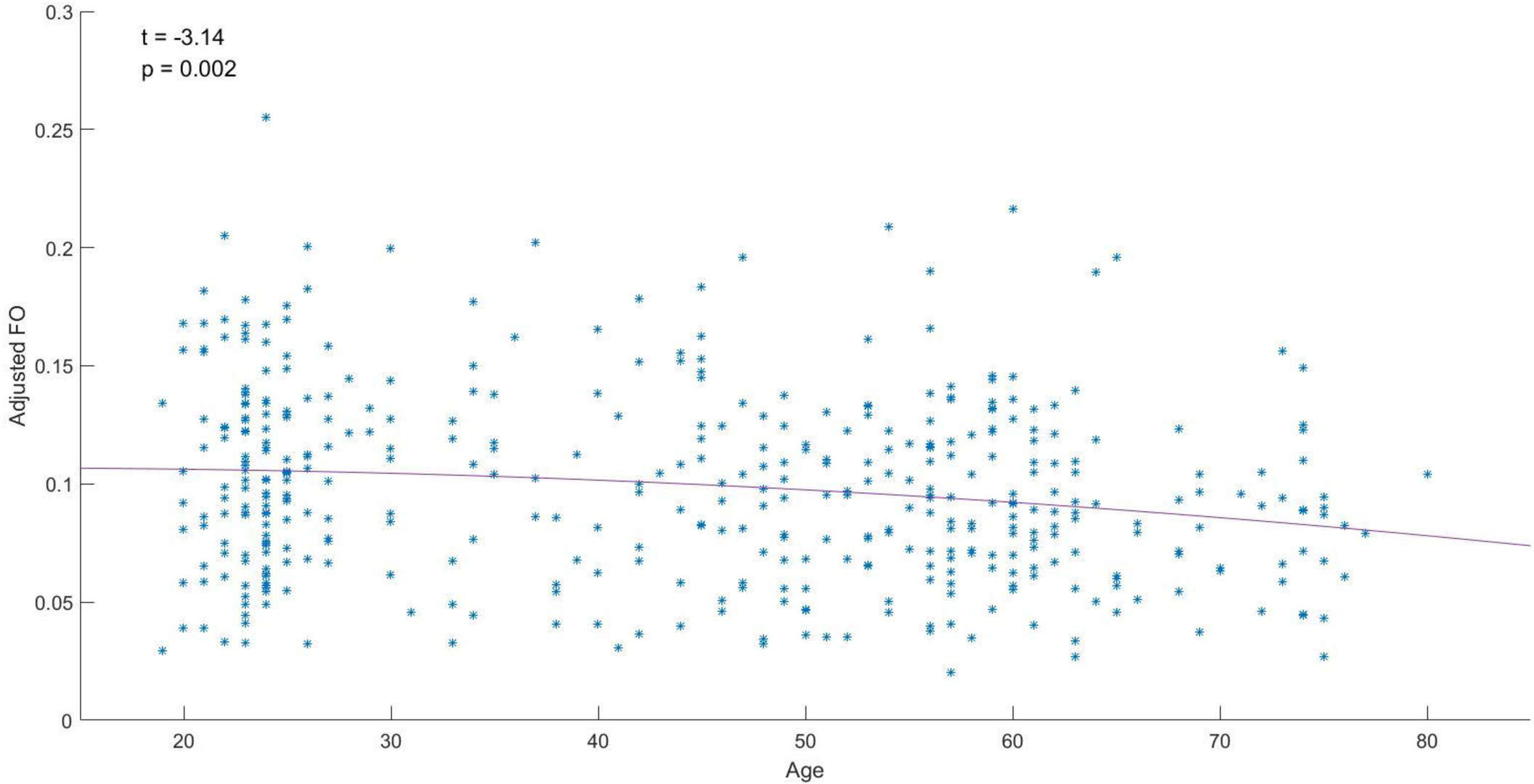
t = -3.14
p = 0.002
Adjusted FO
Age
0.3
0.25
0.2
0.15
0.1
0.05
0
20
30
40
50
60
70
80

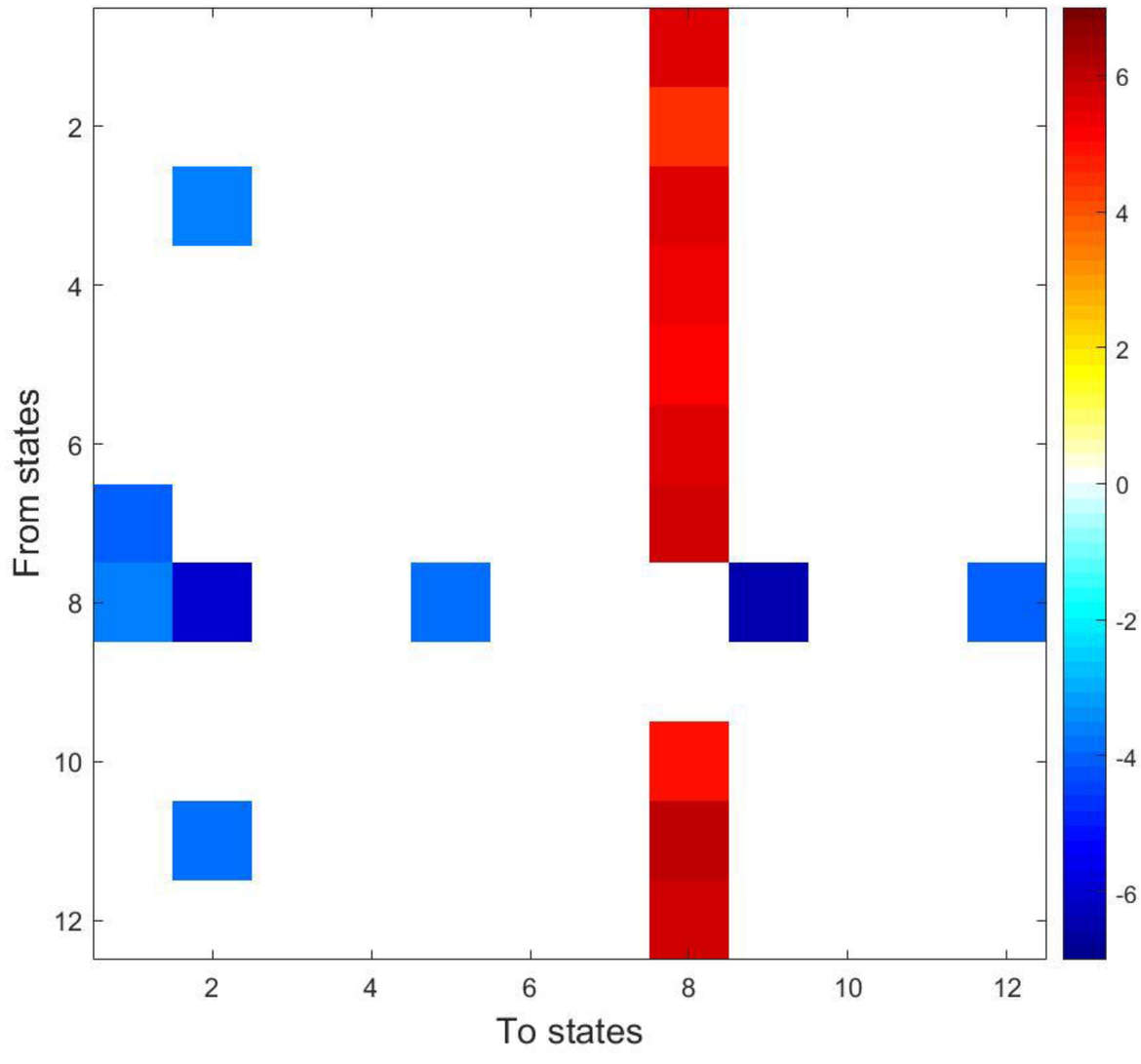
From states
To states
2
4
6
8
10
12
6
4
2
0
-2
-4
-6

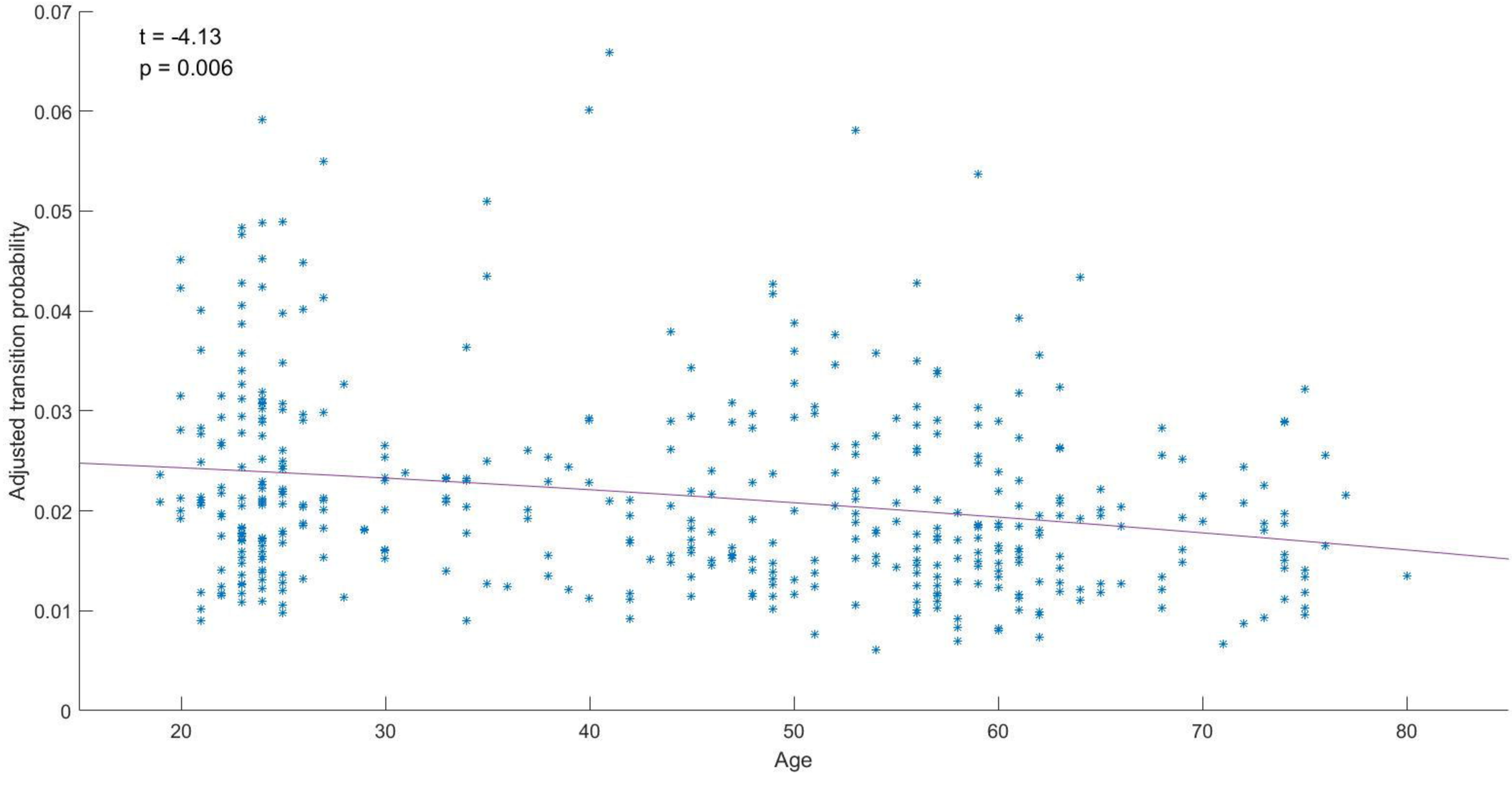
t = -4.13
p = 0.006
Adjusted transition probability
0.07
0.06
0.05
0.04
0.03
0.02
0.01
0
20
30
40
50
60
70
80
Age

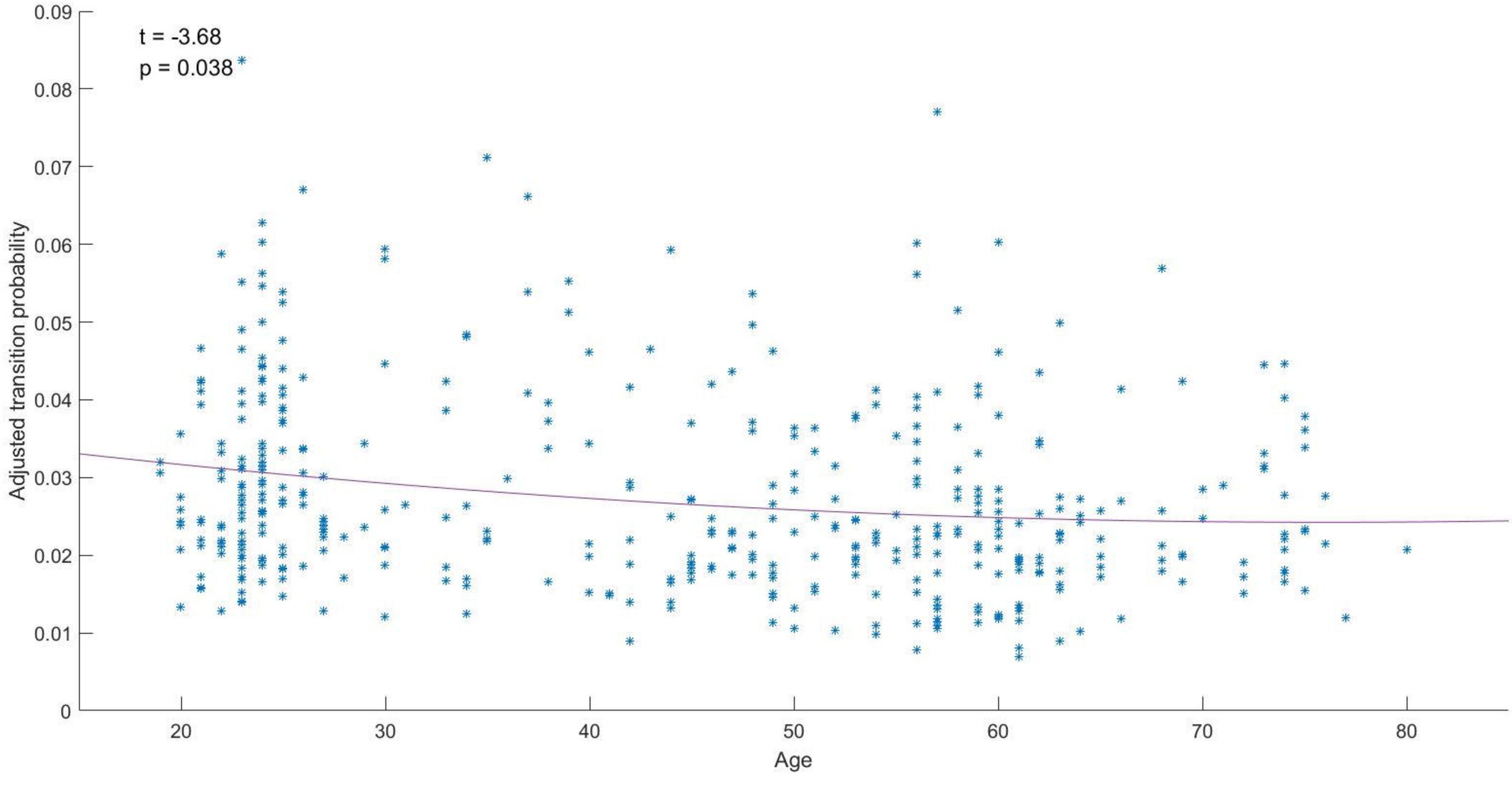
t = -3.68
p = 0.038 *
Adjusted transition probability
0.09
0.08
0.07
0.06
0.05
0.04
0.03
0.02
0.01
0
20
30
40
50
60
70
80
Age

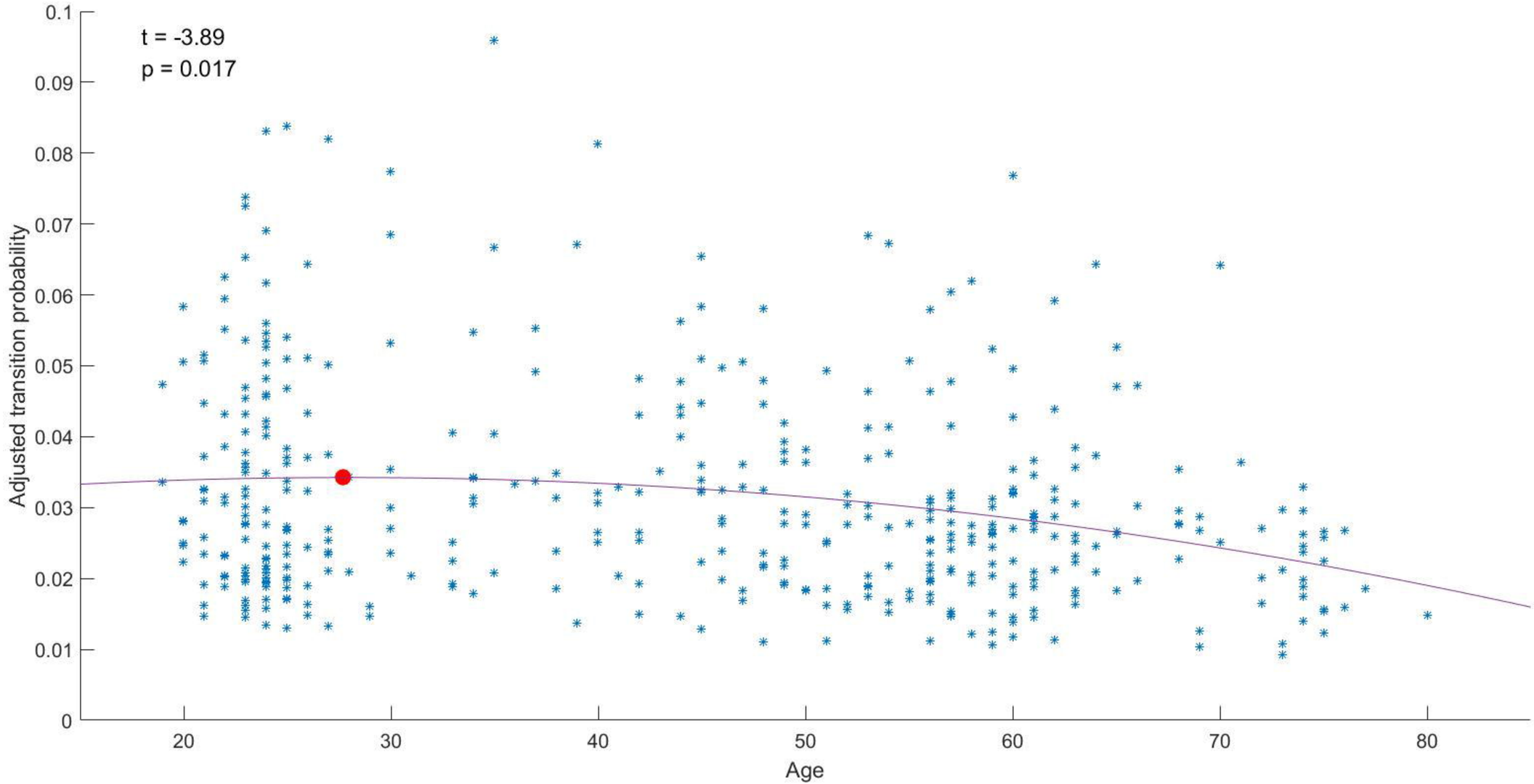
t = -3.89
p = 0.017
Adjusted transition probability
0.1
0.09
0.08
0.07
0.06
0.05
0.04
0.03
0.02
0.01
0
20
30
40
50
60
70
80
Age

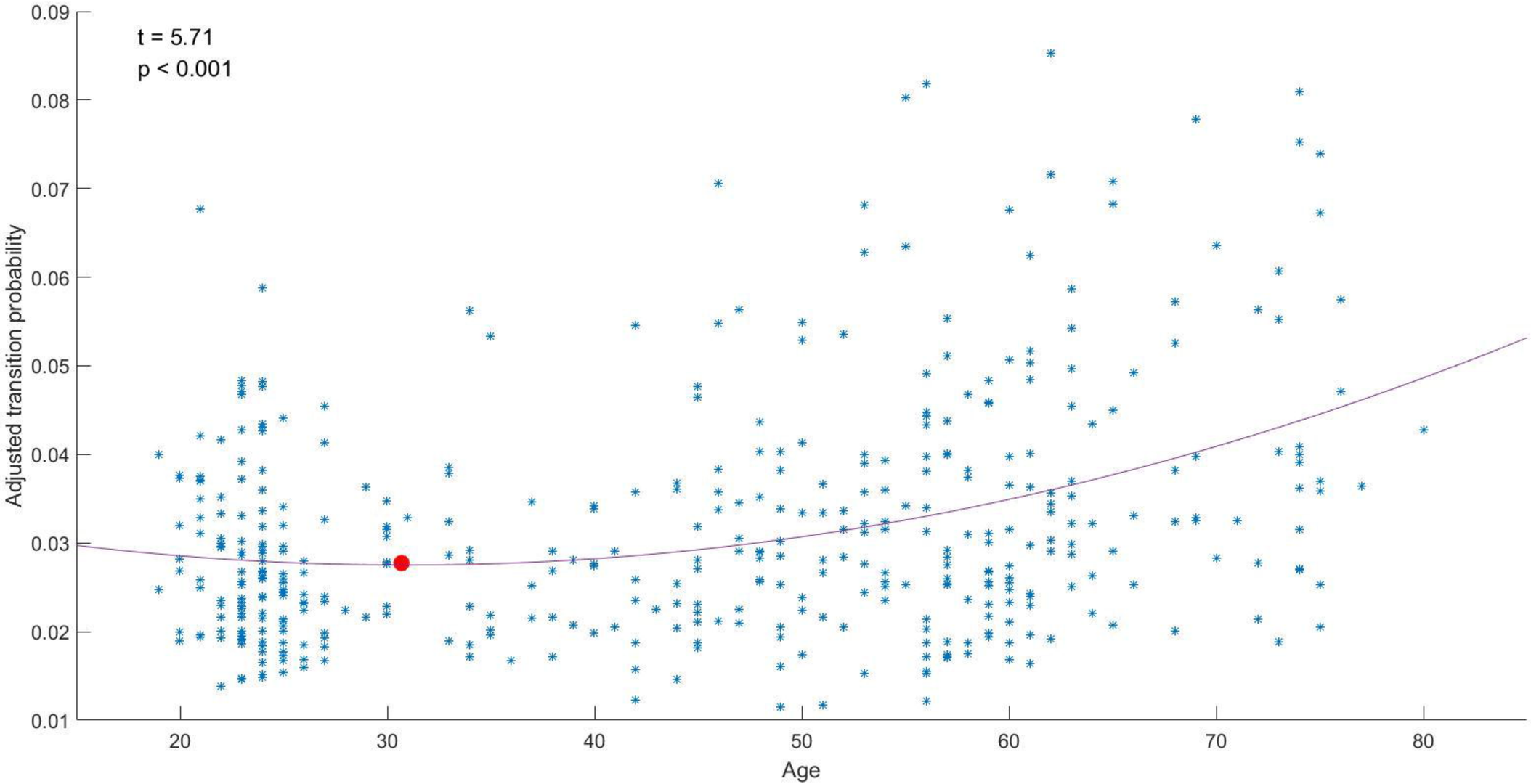
t = 5.71
p < 0.001
Adjusted transition probability
0.09
0.08
0.07
0.06
0.05
0.04
0.03
0.02
0.01
20
30
40
50
60
70
80
Age

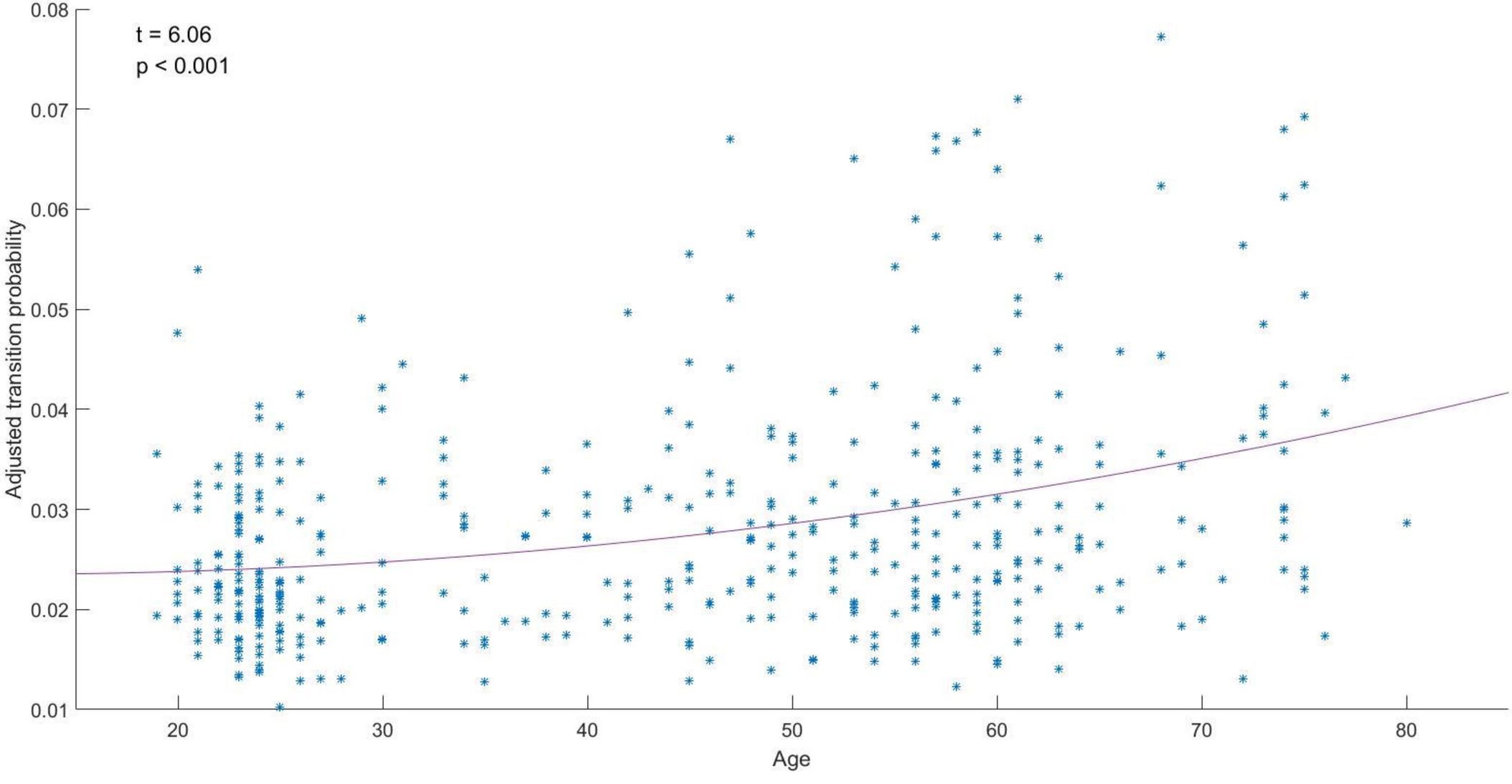
t = 6.06
p < 0.001
Adjusted transition probability
0.08
0.07
0.06
0.05
0.04
0.03
0.02
0.01
20
30
40
50
60
70
80
Age

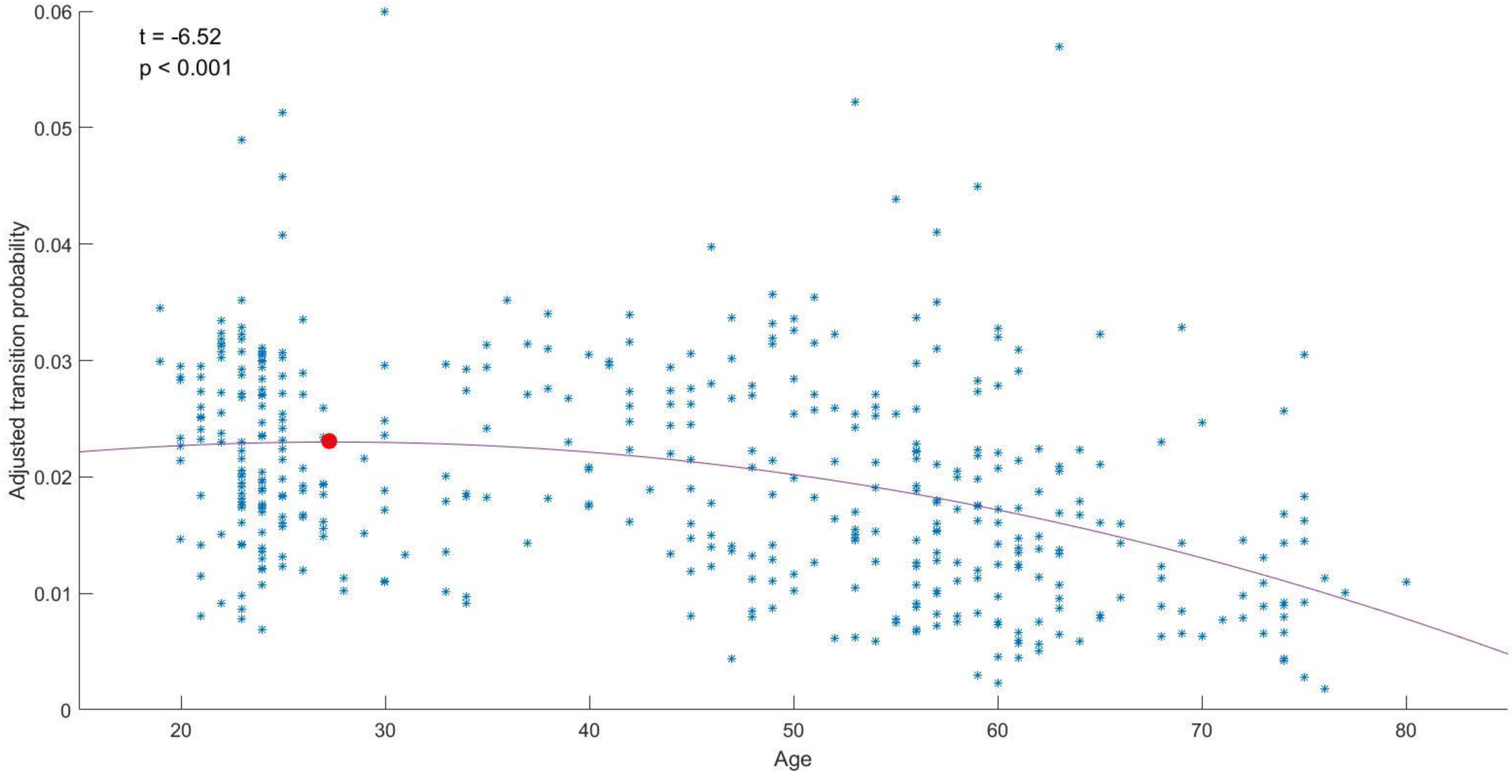
t = -6.52
p < 0.001
Adjusted transition probability
0.06
0.05
0.04
0.03
0.02
0.01
0
20
30
40
50
60
70
80
Age